CellPress REVIEWS

Review

Electroluminescence of Perovskite Nanocrystals with Ligand Engineering

Jinwoo Park,[1] Hyun Myung Jang,[2] Sungjin Kim,[1] Seung Hyeon Jo,[1] and Tae-Woo Lee[1,3,4,*]

Light-emitting diodes (LEDs) based on metal halide perovskite nanocrystals (MHP NCs) have been rapidly developed to reach external quantum efficiencies of up to 22% with their defect-tolerant nature and extremely high color purity (full width half maxima <25 nm) that are superior to traditional inorganic colloidal quantum dots. However, highly dynamic binding of ligands impedes further increase in efficiency and induces intrinsic instability. In this review, we discuss the light emission in MHP NCs, surface chemistry regarding the surface termination of MHP crystal, and the binding of ligands to crystals. We also discuss strategies to overcome the instability of ligands to improve efficiency and stability of MHP NCs and finally achieve high efficiency of their LED devices.

Highlights

Colloidally synthesized metal halide perovskite nanocrystals (MHP NCs) have a unique defect-tolerant nature, with extremely high color purity and high photoluminescence quantum yield, affording them high potential as light sources in next-generation displays.

The dynamics of organic ligands on the MHP NC surface limits efficiency and stability, and their insulating nature impedes charge transport in MHP NC light-emitting diodes. Increase in efficiency and stability of MHP NC light-emitting diodes requires tight-bound passivation with minimal content of insulating components.

Surface engineering that exploits understanding of surface chemistry and binding state of ligands is critical for surface passivation and efficient charge transport to achieve efficient and stable light-emitting diodes.

Perovskites for Next-Generation Optical Sources

In display technology, color gamut defines the range of color that a display can express. Accuracy of reproduction of the natural color in the display has become a critical evaluation indicator, so the importance of color gamut has increased and, accordingly, standards to evaluate it have been developed; examples include National Television System Committee (NTSC), sRGB, Adobe RGB, and Rec. 2020 [1]. The most recent standard of color gamut is Rec. 2020; it was proposed for ultrahigh-definition television by the International Telecommunications Union in 2012 [2]. Rec. 2020 comprises almost 100% of all **Pointer's gamuts** (see Glossary) and enables accurate representation of the light reflected from surfaces. To achieve Rec. 2020 standards in the display, high color purity of each red, green, and blue light with appropriate peak wavelength (red ~630 nm, green ~530 nm, and blue ~465 nm) must be achieved, but these requirements are not achieved by conventional organic emitters.

Metal halide perovskites (MHPs) are ionic compounds with ABX_3 structure [A = monovalent cation (e.g., methylammonium, formamidinium, Cs^+), B = metal cation (Pb^{2+}, Sn^{2+}), X = halide anion (Cl^-, Br^-, I^-)]. They are promising future emitters as an alternative to organic emitters for next-generation optoelectronic devices with high color purity of narrow full width half maximum (FWHM) <25 nm [3–5], facile tuning of emission wavelength (400 to 800 nm) [6,7], and high carrier mobility [8,9]. Owing to the excellent optical and electrical properties, MHP light-emitting diodes (PeLEDs) have been widely studied since the demonstration of room-temperature bright electroluminescence [3,4] and the first efficient electroluminescence [5]; their **external quantum efficiency (EQE)** has been increased to >20% [10–15].

Colloidal synthesis is an effective strategy to prepare high-quality MHP crystals with high **photoluminescence quantum yield (PLQY)** [7,16–18]. In this method, MHPs are crystallized in the solution stage with the assistance of organic ligands [19,20] that restrict the growth of MHP crystals and stabilize them to increase their dispersion stability. The size of MHP nanocrystals (NCs) can be easily controlled by using organic additives or ligands [5,7,18,21], so exciton dissociation as a result of the small **exciton binding energy** of MHP can be overcome [5,7]. Furthermore, colloidal synthesis offers reproducibility and scalability. Unlike traditional

[1]Department of Materials Science and Engineering, Seoul National University, 1 Gwanak-ro, Gwanak-gu, Seoul 08826, Republic of Korea
[2]Research Institute of Advanced Materials (RIAM), Seoul National University, 1 Gwanak-ro, Gwanak-gu, Seoul 08826, Republic of Korea
[3]School of Chemical and Biological Engineering, Seoul National University (SNU), Seoul 08826, Republic of Korea
[4]Institute of Engineering Research, Research Institute of Advanced Materials, Nano Systems Institute (NSI), BK21 PLUS SNU Materials Division for Educating Creative Global Leaders, Seoul National University, 1 Gwanak-ro, Gwanak-gu, Seoul 08826, Republic of Korea

*Correspondence:
twlees@snu.ac.kr (T.-W. Lee).

inorganic colloidal quantum dots (cQDs), facile room-temperature synthesis is even possible for MHP NC and, thus, large-scale synthesis can be achieved. Up to liter-scale or gram-scale synthesis have been reported and further larger-scale synthesis is expected to be possible [22,23]. Also, the crystallization of the MHP is terminated in the solution state, so the effect of the environment in coating process on the MHP crystal is reduced. MHP NCs can be coated reproducibly on a large scale onto various substrates [24–26]. Therefore, MHP NCs have a high potential to be commercialized as next-generation optical sources that fulfill the Rec. 2020 standard.

Numerous reports of MHP NCs and their application in PeLEDs have been reported (Figure 1A). General and practical strategies to increase the efficiency of LEDs include surface passivation to reduce surface defect-related nonradiative recombination and improving charge transport in MHP NCs (Figure 1B) [27]. Surface-related engineering of MHP NCs using surface halide exchange or surface ligands has enabled the rapid increase of EQE to 21.3% in red [10] and 22% in green [109].

Another important major hurdle for the commercialization of PeLEDs is operation stability. State-of-the-art efficiency of PeLEDs is now compatible with that of organic and cQD LEDs, their operation stability is lagged behind. One of the most critical issues in PeLED stability is a mobile ion. Mobile ions in MHP crystal can easily migrate under the electric field; **ion migration** in MHP can result in easy degradation of MHP crystal and instability of the emission wavelength [29]. In polycrystalline MHP, grain boundary is the major channel for ion migration [30]. On the contrary, in MHP NCs, organic ligands on their surface can efficiently prevent the ion migration [20]. However, when proper passivation of the MHP NC surface by organic ligands is not done, possibly due to their dynamic nature, interparticle ion migration from the surface of MHP NC can reduce the luminance efficiency; this can be especially more plausible in small MHP NC due to the large specific area. Therefore, ligand engineering, including control of ligand density, bulkiness, and binding motif is essential for PeLED stability as well as their efficiency.

Emission in MHP NCs

MHP NCs are nanometer-scale MHP crystals, generally surrounded by organic ligands; this is a similar structure to that of cQDs. Although cQDs and MHP NCs are similar in structure and both have excellent optical properties (high PLQY, narrow FWHM), their optical properties occur by

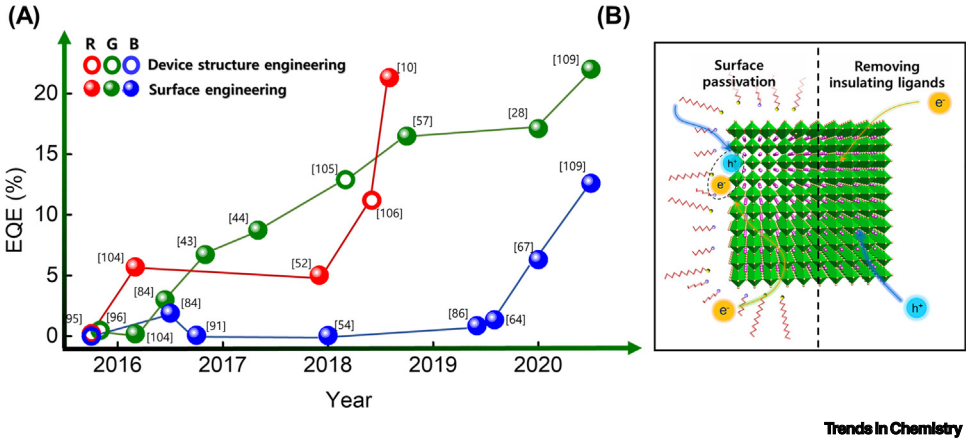

Figure 1. Development of Perovskite Light-Emitting Diodes Using Metal Halide Perovskite (MHP) Nanocrystals (NCs). (A) External quantum efficiency (EQE) development of red-, green-, and blue-emitting MHP NC LEDs. Data acquired, with permission, from [10,28,43,44,52,54,57,64,67,84,86,91,95,96,104–106,109]. (B) Schematic representation of surface engineering [surface passivation (left) and removing insulating ligands (right)].

Glossary

Exciton binding energy: E_B, minimum energy needed to separate an exciton into free charge carriers.

Exciton Bohr diameter (D_B): two times exciton Bohr radius (R_B), which is the most probable distance between the electrostatically bound electron and hole in a pair. In quantum size $<D_B$, excitons experience a non-negligible quantum-confinement effect, so they have discrete energy levels.

Excitonic recombination: recombination of the electrostatically bounded electron–hole pair (exciton) without dissociation into free charge carriers. Excitonic recombination as a proportion of free-carrier recombination is determined by exciton binding energy. With small exciton binding energy, the exciton can be easily dissociated by thermal energy into free carriers before the recombination.

External quantum efficiency (EQE): in light-emitting diodes (LEDs), refers to the number of photons emitted out of the device as a percentage of the electrons that are injected into the device [% ph/el]. EQE with a given electroluminescence spectrum can be calculated from total radiant power [W] in an integrating sphere, or from radiance [W m^{-2} sr^{-1}] in a goniometric measurement set-up.

Ion migration: movement of charged particles. Ion migration in ABX_3 metal halide perovskite usually refers to movement of a component (e.g., A^+, B^{2+}, X^-) of the ionic crystal under light stimulation or electrical bias. Ion migration can be the major reason for degradation of perovskite optoelectronic devices.

Photoluminescence quantum yield (PLQY): the number of photons emitted as a percentage of the number of photons absorbed by the material.

Pointer's gamut: gamut of colors that the human eye can detect in light reflected from the surface of a material. Displays that emit 100% of the Pointer's gamut can reproduce all the colors of a real surface of the materials that do not contain a fluorescent component.

distinct mechanisms. Typically, emission in cQDs exploits the quantum confinement effect [31,32]. To achieve high PLQY in cQDs, they should have a diameter smaller than **exciton Bohr diameter (D_B)**, so their emission is ascribed to a strong confinement regime. In this regime, exciton interaction in cQDs is highly dependent on the size of the particles. Thus, the color purity of the cQD ensemble is critically dependent on their size distribution.

However, the emission in MHP crystals beyond D_B is dependent on its crystal structure [33,34]. Even though they can easily have a high concentration of defects due to the low formation energy of point defects such as halide vacancies, most of the defects are located within the valence band and conduction band [34,35]. Therefore, the bulk defect states in MHP crystals mostly do not induce additional nonradiative recombination and the surface defects can easily be passivated by simple chemical modification such as use of ligands in NCs. As a result, MHP NCs can show high color purity and near-unity PLQY, even without encapsulation by an epitaxial shell, which is essential to achieve high PLQY in cQDs [36,37].

Although the MHP NCs do not need the epitaxial shell, appropriate passivation of the surface by ligands is still essential because of surface defect formation in NCs; most defects in MHP NCs are located on their surfaces and even deep traps can be generated there [38]. The defect densities of small NCs are influenced by a large specific surface area and complex chemical interaction between ligands and solvent [38].

The size of MHP NCs should be controlled, considering the range of D_B, which in MHP is from 7 to 10 nm when the X-site halide is Br^-, and can be slightly affected by the A-site cation [7,21,39]. As the size of the particles decreases, their luminescence efficiency is influenced by two conflicting factors: (i) increasing spatial confinement of the exciton to facilitate radiative recombination; and (ii) increasing nonradiative recombination at surface trap sites due to the increase in surface-to-volume ratio. The defect-tolerant nature of MHP allows sufficiently large spatial confinement to achieve high PLQY while minimizing the effect of surface traps. When MHP NCs are larger than D_B, the quantum confinement effect is negligible (weak), so emission is nearly unaffected by the size and can show high color purity with high PLQY, independent of size [21]. Thus, even without precise control of the size distribution during synthesis, the emission spectra do not broaden, so FWHM can be reduced at low cost (Figure 2A) [21,23]. Especially when MHP NCs are larger than critical diameter (D_C), which is highly dependent with D_B (Box 1), the quantum confinement effect is nullified.

If the dimension of the MHP crystal is reduced below that of the D_B, it becomes a QD (Figure 2B) [21,40,41]. In this regime, the MHP crystal has emission dynamics that are similar to those of cQDs. Therefore, beyond facilitating the **excitonic recombination** in small particle size, further reduction in the size of the MHP NCs can blue shift the emission wavelength without any change in their composition. The bandgap of MHPs can also be easily tuned by controlling the halide composition, but when halides in an MHP crystal are mixed, they can segregate spatially and shift the emission wavelength under electrical bias [42]. Therefore, color tuning that exploits quantum confinement can be an effective alternative strategy to precisely control the emission wavelength and is particularly useful to achieve stable blue emission [40,41].

Overcoming the Insulating Nature of Organic Ligands

Controlling the Charge Transport Properties of Ligands

The crystal size in the solution state during the synthesis process can be easily tuned by controlling the density, chain length, and functional groups of the organic ligands. They stabilize the surface of the MHP NCs to reduce the number of possible nonradiative recombination sites on the

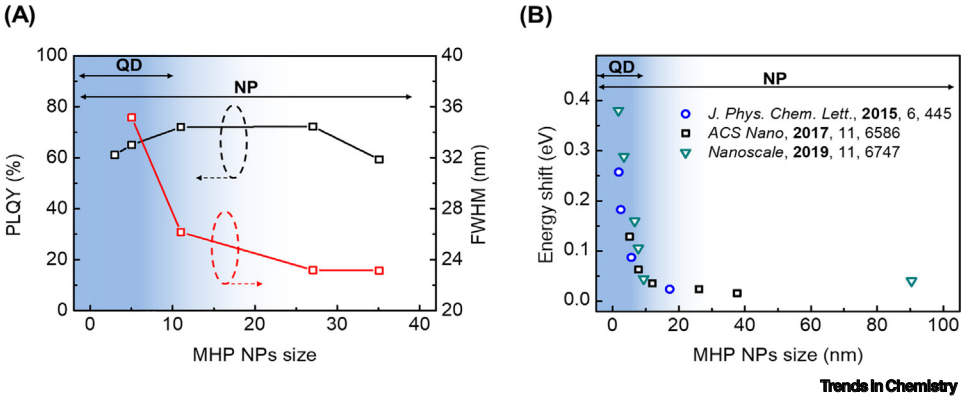

Figure 2. Quantum Confinement Effects in Metal Halide Perovskite (MHP) Nanocrystals (NCs). (A) Photoluminescence quantum yield (PLQY) and full width half maximum (FWHM) shift, reproduced, with permission, from [21]. (B) Emission peak energy shift of $MAPbBr_3$ MHP NCs versus MHP NC size with labeled quantum dot (QD) and NC regimes. Data acquired, with permission, from [21,107,108] and reproduced, with permission, from [107].

surface of the MHP crystal [43,44]. Furthermore, organic ligands impede ion migration and reduce the number of defects that it can cause [45,46]. Besides, in MHP NC thin films, ligand length and density on the MHP NC surface can affect morphological and electronic properties. Oily ligands (e.g., oleylamine) hinder the smooth formation of MHP NC thin films. Also, longer carbon chains in the organic ligands can impede charge transport and reduce the coupling among QDs (Figure 3A). Thus, to achieve efficient carrier injection and radiative recombination, the design of ligands in MHP NCs should consider both chemical and electrical properties.

Therefore, the chain length and the density of ligands in MHP NCs must be optimized. Insufficient length of ligand (propylamine) could not provide the stability of MHP NCs in solution and led to very low PLQY (Figure 3B) [47]. However, appropriate ligand length can achieve a good trade-

Box 1. Calculation of the Critical Diameter

The energy E_{exc} of confined excitons in a spherical QD can be obtained by considering that E_{exc} is the sum of two distinct contributions: (i) the energy E_{sc} of (asymptotically) strongly confined individual *e* and *h* particles, and (ii) the spatial *e-h* correlation energy E_{corr}. In spherical NCs of radius *R*, the exciton energy above the bandgap can be written as

$$E_{exc} = E_{sc} + E_{corr} = \frac{\hbar^2\pi^2}{2\mu R^2} - \frac{C_1 e^2}{4\pi\varepsilon_o\varepsilon_r R} + E_{corr}$$

where μ denotes the reduced mass of an exciton under a strongly confined state [100–103]. The first two terms represent the kinetic and Coulombic potential energies of a strongly confined exciton, where $C_1 = 1.786$ is theoretically optimized constant [100,101]. Under a strongly confined condition, the *e-h* correlation in an exciton collapses, so $E_{corr} \rightarrow 0$.Under this condition, one can immediately deduce the critical diameter D_C for the PL blue shift from Equation I as

$$D_C = \frac{4\pi\varepsilon_o\varepsilon_r\hbar^2\pi^2}{2C_1\mu e^2} = \frac{\pi^2}{2C_1}D_B.$$

D_C corresponds to the onset of the PL blue shift and can be theoretically correlated with the onset of rapid increase in the correlated exciton mass. D_C is also exciton Bohr diameter D_B with a proportionality constant of $\pi^2/(2C_1) \approx 2.75$ [103]. For $MAPbBr_3$, ~10 nm was deduced for the boundary between quantum and nonquantum confined NCs. The assumption that this boundary size is equal to D_B is qualitatively supported by Equation II because the onset of PL blue shift indicates that $D_C \approx 30$ nm [21]. The proportionality constant can be significantly reduced if including $E_{corr}(R \rightarrow 0)$ is considered in the account.

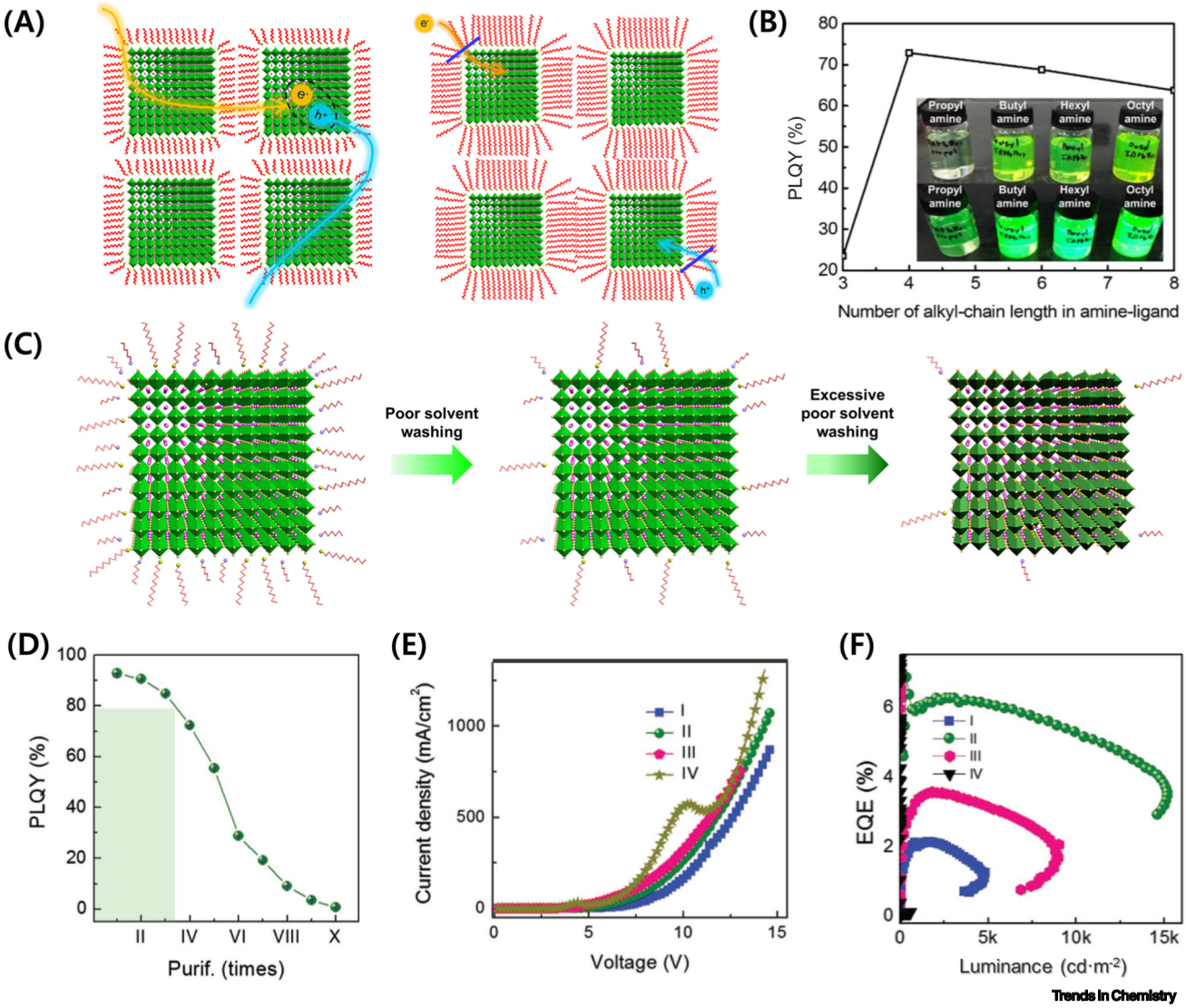

Figure 3. Overcoming the Insulating Nature of Ligands in Metal Halide Perovskite (MHP) Nanocrystals (NCs). (A) Schematic representation of charge transport in MHP NC with varying ligand lengths. Efficient carrier injection and transport to form excitons in short-ligand MHP NCs (left) and impeded transport in long-ligand MHP NCs. (B) Photoluminescence quantum yield (PLQY) of MHP NCs with various ligand chain length and their photograph under ambient and UV light (inset), reproduced, with permission, from [48]. (C) Schematic representation of the reducing ligand density in washing process and degradation by excessive washing process. (D) PLQY change, (E) current density increase, and (F) device efficiency change with multiple washing processes. Adapted, with permission, from [43].

off between surface trap-assisted recombination and confinement of excitons to maximize PLQY, to stabilize the phase of MHP crystal, and to improve charge injection and increase charge-transport capability (Figure 3B) [48,49]. Short, conductive aromatic ligands can overcome the insulating nature of carbon chain ligands. Aromatic ligands can allow delocalization of the electronic wave function and facilitate charge transport. MHP NCs with aromatic ligands can be achieved both by direct synthesis [50–53] or by solid-state ligand exchange [53,54]. The EQE of PeLEDs was boosted from 2.45% to 14.08% by two-step ligand engineering to replace the long insulating ligand; addition of phenethylamine during synthesis and then solid-state ligand exchange using phenethylammonium iodide [53].

Inorganic ligands such as metal halides (e.g., PbI_2, CsI) can be ideal to replace insulating carbon chains and are effective in conventional cQDs [55,56]. Ligand-exchange strategies in cQDs use polar solvent and cannot be directly applied to MHP NCs, but inorganic metal bromide has been used to partially replace organic ligands [57,58]. MHP NCs with inorganic ligands showed increased conductivity and simultaneous effective passivation of the NC surface increased PLQY and colloidal stability [57]. With increased transport and passivation, PeLEDs based on $ZnBr_2$-passivated MHP NCs showed improved EQE from 10.7% to 16.48% [57]. This strategy of using metal bromide inorganic ligands can be applied generally; various metal bromides (e.g., $ZnBr_2$, $MnBr_2$, $GaBr_3$, $InBr_3$) are effective to increase the charge transport in MHP NC films [57].

Postsynthesis Washing Treatment

Charge injection to the MHP NCs layer also can be increased by a postsynthesis washing treatment. Excess ligand presence during synthesis can hinder charge transport, so the excess ligand must be removed. However, conventional surface treatment methods that use a polar solvent (as for cQDs) can cause the dissolution or phase transformation of MHP crystals [59]. Therefore, only very restricted and delicate methods are feasible to manipulate the ligand density of MHP NCs.

A practical method to remove the excess ligands is a purification process that uses a poor solvent that cannot disperse MHP NCs (e.g., methyl acetate, ethyl acetate, butanol, or pentanol) (Figure 3C). After the synthesis of the MHP NCs, a poor solvent is added to the colloidal solution that is then centrifuged to precipitate MHP NCs [43]. Precipitated MHP NCs can be washed further with a poor solvent in a multiple-stage purification process [43,44,59]. During the multiple-stage purification process, the ligand density in the MHP NC surface can be gradually decreased, resulting in increased charge transport through the MHP NC films. The morphology of the film can be smoothed by reducing the content of oily ligands [43]. Ligand removal with poor solvent(s) is also practical to increase dot-to-dot charge transport in the solid phase after film formation [60–63].

However, during the purification process, a poor solvent can quickly degrade the ionic crystals of MHP [43]. Also, excessive removal of the ligands leads to insufficient passivation of the surface defects and, as a result, can cause poor colloidal stability and facilitate nonradiative recombination (Figure 3C). For example, PLQY was only slightly reduced from 92% to 90% with two cycles of purification with ethyl acetate, but was significantly decreased by subsequent cycles, to <60% PLQY after the fifth cycle (Figure 3D) [43]. Therefore, the purification solvent and number of purification cycles must be optimized for efficient PeLED fabrication. As the number of purification cycles increases, current density in PeLEDs increases (Figure 3E), but the maximum EQE and luminance were optimized with two cycles of purification due to the trade-off between charge transport and internal quantum yield (Figure 3F). The dielectric constant is correlated with the effectiveness of the purification solvent [59]. In the dielectric constant range of 5–10, poor solvent effectively reprecipitates the MHP NCs without critical degradation of the emission properties. Multiple washings in diglyme, which is a poor solvent with a low dielectric constant (7.23), achieved highly efficient PeLEDs (EQE_{max} = 8.8%) [59].

Additional halide source treatment can prevent critical degradation during the washing process. One method exploits a mild reaction that uses thionyl halide as an additional halide source. The thionyl halide reacts with bulky acid and amine ligands and replaces halide anions [64]. The halide in thionyl halide can prevent the generation of halide vacancies, which is similar to occupation of halide vacancies by the halogen in metal halide [65,66]. Thus, repeated washing process without critical degradation was possible and bulky ligands could be removed completely [64]. This use of additional halide source maintained PLQY of MHP NCs >80%, whereas the conventional

washing process reduced PLQY to <40% after four cycles. Passivation of halide vacancy can be also achieved by organic psuedohalides without unwanted peak shift due to the halide exchange [67,68]. Nonpolar solvent-soluble organic psuedohalides, *n*-dodecylammonium thiocyanate filled the halide vacancy in blue-emitting $CsPb(Br_xCl_{1-x})_3$ NCs and enabled EQE of 6.3% with peak emission wavelength of 471 nm [67].

Surface Chemistry and Ligand Binding of MHP NCs

Surface Stoichiometry

Knowledge of the effects of surface chemistry and binding state of ligands can help to increase understanding of the emission dynamics and give insight into ways to increase the luminance of MHP NCs. Ligands of the NC can be classified according to the binding of ligands to the NC surface. L-, X-, and Z- type ligands are distinguished by the number of electrons (2, 1, and 0, respectively) that are donated to the metal to form a bond to the surface of the NC according to the covalent bond classification method (Figure 4A) [69,70]. Therefore, typical Lewis acids can act as Z-type ligands [e.g., $Cd(O_2CR)_2$, $CdCl_2$ (R=alkyl)]; on the contrary, Lewis bases can act as L-type ligands [e.g., NH_2R, PR_3 (R=alkyl)] [70]. It is also notable that the classification of the same ligands can be different if the binding motif to the NC surface changes in the different environment [71]. In MHP NCs that are synthesized by a typical method that uses an acid and amine [7,21], the surface has a Br-rich stoichiometry [72–75]. X-ray photoelectron spectroscopy analysis using various photon energies E_P can define the stoichiometry in MHP NCs in the core and on the surface of NCs [75]. In $CsPbBr_3$ NCs, the Pb/Cs ratio was almost constant regardless of E_P, but at E_P = 650 eV, the Br/Cs ratio was 5, which is larger than the expected ratio of 3; however, E_P > 1100 eV the ratio saturated at 3 (Figure 3B) [75]. This dependence of atomic ratio on E_P indicates that a Br-rich layer surrounds the $CsPbBr_3$ NCs.

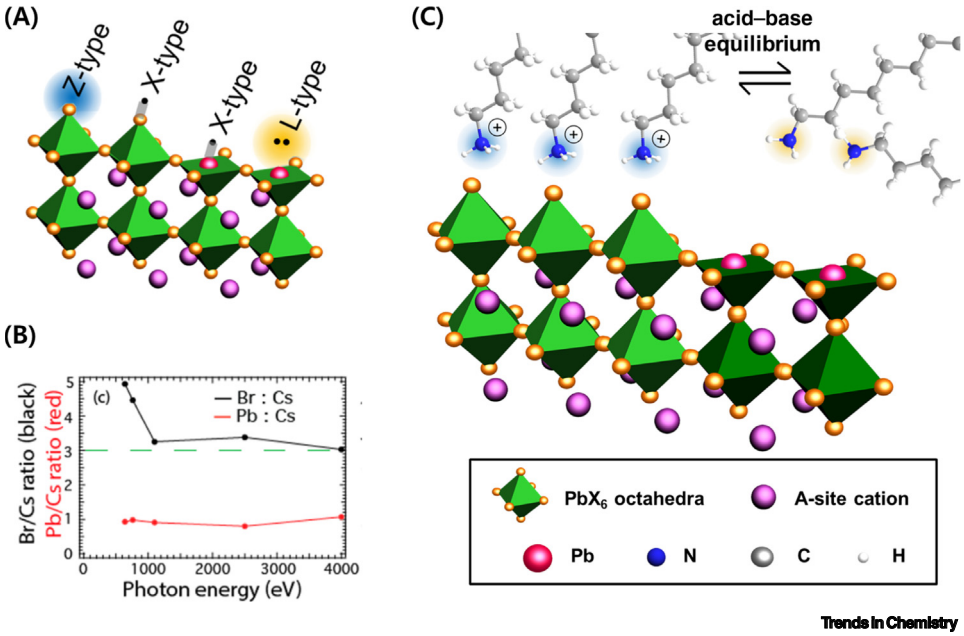

Figure 4. Halide-Rich Surface Termination and Dynamic Binding of Ligands on Metal Halide Perovskite (MHP) Nanocrystals (NCs). (A) Schematic representation of the covalent bond classification of ligands. (B) Atomic ratio in MHP crystal calculated from X-ray photoelectron spectroscopy analysis with different photon energy, adapted, with permission, from [75]. (C) Schematic representation of bonding of protonated amine on bromide-rich surface of MHP crystal and desorption and consequent undercoordinated Pb defect due to the acid-base equilibrium.

The Br-enriched surface layer has a larger bandgap than the core MHP NCs and can form a band alignment that resembles a quantum well [74]. Therefore, excess Br in the surface can self-passivate defects, confine excitons in the MHP crystal, and facilitate radiative recombination. The self-passivation effect by the Br-rich surface agrees well with results of experiments [74] and first-principles calculations [34], that a halide-rich environment during synthesis can increase the efficiency of MHP NCs.

Dynamic Ligand Binding and Halide Exchange

On MHP NCs that have a Br-rich surface, amine and acid ligands tend to form ionic bonds rather than tight bonds that have a highly covalent characteristic. In the presence of the acid, amine ligands undergo a protonation reaction to form an organic ammonium cation, which can bind with surface bromide to form ammonium bromide [76,77]. The ammonium bromide terminations of MHP NCs can be either ammonium cation bound to bromide (a Z-type ligand) or ammonium bromide bound to Pb (X-type). Ionic characteristics of crystal and ligands in MHP NCs are related to the highly dynamic nature of ligand binding. Nuclear Overhauser effect spectroscopy confirmed that the amine ligands bind to Br-rich surface, and the diffusion coefficient of bound amine ligands calculated from diffusion ordered spectroscopy data was significantly larger than the expected value of a bound state; this difference indicates that ligand binding in MHP NCs is highly dynamic (Figure 4C) [77–79].

The dynamic ligand nature of the MHP NCs results in dynamic halide exchange obtained by using an additional halide source. Organic ligands surrounding MHP crystal cannot form an adequate diffusion barrier, so halide ions from the MHP crystal and additional source mix easily to form a mixed-halide MHP crystal within seconds. This halide-exchange reaction can be exploited to tune the bandgap and photoluminescence (PL) emission wavelength by using ammonium halide [6,10,80,81], metal halide [6,81], haloalkane [82], or MHP NCs with different halides [6]. This unique property resulting from the instability of ligands in MHP NCs has been exploited in applications such as photodetectors [80], color patterning [82], and LEDs [10].

Strengthening the Ligand Binding for PeLED Application

Under the dynamic binding ligand nature of MHP NCs, amine ligands are in acid-base equilibrium with acid ligands or bromide anion to form the chemical products that cannot react with the Br-rich surface of MHP NCs (Figure 4C) [77,83]. Desorption of ligands due to acid-base reactions can leave halide vacancy defects or induce aggregation between MHP NCs to lower their colloidal stability and structural stability. Ligand detachment can lead to formation of undercoordinated Pb ions on the MHP surface, which acts as deep traps [38]. Therefore, to ensure efficiency and stability of MHP NCs, the acid-base reaction of ligands must be constrained.

Quaternary ammonium [e.g., didodecyldimethylammonium halide (DDAX, X = Cl, Br, I)], can interact with a halide-rich surface without protonation and does not undergo acid-base reaction. DDAX can increase the efficiency and the stability of MHP NCs, so it can be used as an alternative to alkylamine ligands (Figure 5A) [44,83–88]. During both direct synthesis and postsynthesis ligand exchange, DDAX works to increase the efficiency of LEDs by passivating the MHP NC surface, preventing aggregation, smoothening the film morphology, and enabling reduction in ligand density [85,87,88]. Zwitterionic ligands are a very effective form of quaternary ligand [83,89]. The combination of a quaternary ammonium and an acid functional group in a single ligand can efficiently replace the acid and amine pairs and improve chemical durability. MHP NCs capped with DDAX have considerably lower ligand diffusion coefficient than MHP NCs capped with aliphatic ammonium and carboxylate; this difference indicates tighter binding of NC to DDAX than to ammonium and carboxylate [90]. Density functional theory calculations suggested that the

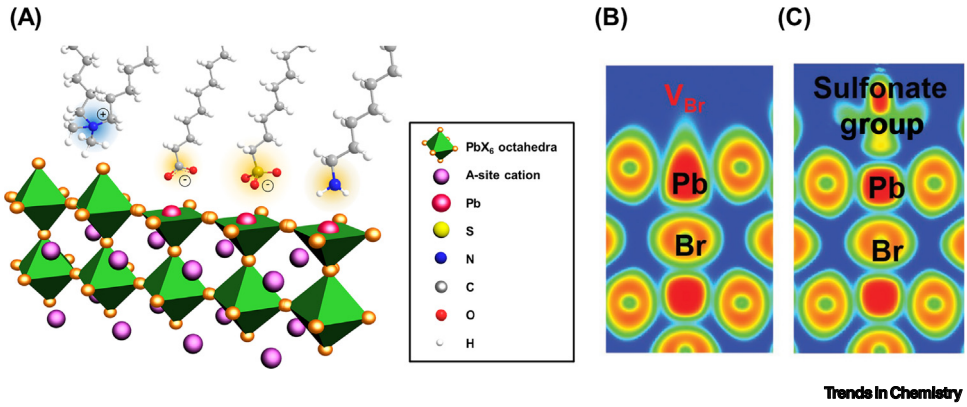

Figure 5. Strategies to Enhance the Binding of Ligands to Metal Halide Perovskite (MHP) Nanocrystals (NCs). (A) Schematic representation of examples of stable binding ligand and binding state (quaternary ammonium [90], oleic acid [91], sulfonic acid [42], and oleylamine [72]). Electron localization function of a $CsPbBr_3$ MHP NC surface (B) without and (C) with strong electron withdrawing groups (sulfonate group), adapted, with permission, from [42].

higher stability with the tighter binding to DDAX than to ammonium and carboxylate does not come from strengthened binding with MHP crystal; however, the quaternary nature of DDAX may be the cause of its weaker interaction with other species, such as solvent [90].

To essentially eliminate the reaction between ligands, a single functional group ligand strategy can be used to synthesize MHP NCs. Since the first demonstration of single ligand synthesis using oleic acid [91], it has been developed by using different types of ligands that can adhere more strongly than oleic acid to the MHP crystal; examples include strongly electron-withdrawing ligands sulfonic acid [42] and phosphonic acid [92], crosslinkable ligand 4-vinyl-benzyl-dimethyloctadecylammonium chloride [93], bidentate ligand 2,2′-iminodibenzoic acid [52], L-type ligand oleylamine [72], and X-type ligand octanethiol (Figure 5A) [72,94]. Notably, a single functional group can replace the surface bromide to form a Pb-ligand bond. Even without a Br-rich surface that self-passivates the MHP crystal [74], the strong interaction between Pb and ligand can effectively preclude the delocalization of electron cloud around the lead atom and thereby stably passivate surface defects on MHP NCs (Figure 5B,C) [42].

Concluding Remarks

Overall, MHP NCs constitute an ideal form of MHP emitter to overcome limitations related to small exciton binding energy of bulk crystals and to retain a high potential to achieve the Rec. 2020 standard. Compared with conventional cQDs, MHP NCs show competitive material price, facile synthesis, and defect-tolerant nature. Because of this high potential, MHP NCs have been intensively studied since 2014, and PeLEDs have been rapidly developed to reach 21.3% EQE in red [10] and 22% EQE in green [109]. Despite the recent rapid development of the MHP NC emitter, device performance of PeLEDs, especially the stability, is still inferior to the state-of-the-art in cQDs (see Outstanding Questions).

The current limitation of MHP NCs is mainly due to the highly dynamic binding of ligands and the fragile ionic nature. During concentrating, diluting, ligand washing, or electrical operations, those features can easily generate defects that can induce nonradiative recombination. Therefore, synthesis or ligand exchange procedure to passivate the MHP crystal with a tight binding and fewer insulating ligands can be effective strategies to increase electroluminescence efficiency. Engineering of the surface ligands must be conducted on the basis of the understanding of the surface chemistry. Controlling the binding state and equilibrium among

Outstanding Questions

What is the ideal diameter for MHP NCs to achieve most efficient and stable emission?

How do ligands that surround MHP NCs affect the operational stability of LED devices in which they are used?

Considering that the ideal wavelengths for practical display applications are 630 nm for red and 450 nm for deep-blue, what is the best way to shift the emission wavelength of devices that have the current state-of-the-art efficiency?

What is the most effective ligand-engineering approach to suppress ion migration in MHP NCs?

How can an epitaxial shell be grown on MHP NC crystals? What would be possible candidates for the shell material?

How can one eliminate halide segregation in mixed halide perovskites and achieve a stable emission wavelength?

Are atomic or fully inorganic passivation possible for MHP NCs, as in cQDs?

How can the intrinsic chemical instability of MHP ionic crystals be overcome? Is perfect isolation of MHP crystals from outer environment (e.g., solvent, oxygen, moisture) possible?

How can the electronic band structure of MHP crystals be adjusted? Are n-doping or p-doping possible?

MHP crystals, ligand and the solvent can overcome the instability of ligands to improve efficiency and stability of MHP NCs and finally be a key factor to achieve high efficiency of their LEDs. Quaternary ammonium halide and zwitterionic ligand can be effective candidates. A single-ligand strategy can also strengthen the bonding, while changing the surface chemistry of MHP crystals.

Efficiency of red- and green-emitting PeLEDs based on MHP NCs have been steadily increased since 2015 (Figure 1A) [95,96]. Research directions to reach the level of state-of-the-art efficiency of organic and cQD LEDs in MHP NC-based LEDs are still actively ongoing. With great attention to increase their efficiency, EQE of red- and green-emitting MHP NC LEDs are expected to reach >23% in 1 to 2 years. Currently, the record EQE of blue-emitting PeLEDs based on MHP NCs is 12.3% [109]. Considering recent rapid improvement of their EQE since 2019, similar exponential EQE increase to those in organic and cQD LEDs could be expected. Judging from this pattern, >15% of blue-emitting EQE could be expected within 1 to 2 years.

For long-term research on MHP NCs, three unresolved major issues are still remaining: (i) deep blue-emitting MHP NCs, (ii) device stability, and (iii) toxicity of Pb. There are two major strategies for blue-emitting MHP NCs: (i) mixing halides (Cl, Br) to increase bandgap, and (ii) size control, which exploits quantum confinement. Each strategy has their intrinsic drawbacks: mixed halides can be segregated to induce emission instability and quantum confined MHP NC have large specific area. Therefore, further research on surface engineering to suppress halide segregation and passivate the surface defects is required. Also, for Pb-free MHP NCs such as $CsSnX_3$, where Sn^{2+} can be easily oxidized to Sn^{4+}, it is more vulnerable to defect generation and thus surface defect passivation can significantly improve their efficiency and stability [97]. Recently, double MHP, in which B^{2+} is substituted with B_1^+ and B_2^{3+}, has gained attention owing to their unique emission characteristics [98]. By doping metal cations into double MHP NCs, high PLQY and stability that is similar or even superior to Pb-based MHP was achieved. Although conventional ligands (e.g., oleic acid, oleylamine) are currently used for their synthesis, surface engineering will be essential for their further application on efficient PeLEDs [99].

In short, further development of surface treatment is crucial to overcome current limitation of MHP NCs. Considering the success of inorganic ligands in cQDs [55,56] and the great enhancement by partial substitution of organic to inorganic ligands in MHP NCs [57], atomic or fully inorganic passivation development could be an effective research direction.

Acknowledgments

This research was supported by the National Research Foundation (NRF) grant funded by the Ministry of Science, ICT and Future Planning, Korea government (Grant No. NRF-2016R1A3B1908431). This research was also supported by the Creative Materials Discovery Program through the NRF (Grant No. 2018M3D1A1058536).

References

1. Soneira, R.M. (2016) Display color gamuts: NTSC to Rec. 2020. *Inf. Disp.* 32, 26–31
2. International Telecommunications Union (2012) *The Present State of Ultra-High Definition Television*, ITU
3. Tan, Z.K. *et al.* (2014) Bright light-emitting diodes based on organometal halide perovskite. *Nat. Nanotechnol.* 9, 687–692
4. Kim, Y.-H. *et al.* (2015) Multicolored organic/inorganic hybrid perovskite light-emitting diodes. *Adv. Mater.* 27, 1248–1254
5. Cho, H. *et al.* (2015) Overcoming the electroluminescence efficiency limitations of perovskite light-emitting diodes. *Science* 350, 1222–1225
6. Nedelcu, G. *et al.* (2015) Fast anion-exchange in highly luminescent nanocrystals of cesium lead halide perovskites ($CsPbX_3$, X = Cl, Br, I). *Nano Lett.* 15, 5635–5640
7. Protesescu, L. *et al.* (2015) Nanocrystals of cesium lead halide perovskites ($CsPbX_3$, X = Cl, Br, and I): novel optoelectronic materials showing bright emission with wide color gamut. *Nano Lett.* 15, 3692–3696
8. Yettapu, G.R. *et al.* (2016) Terahertz conductivity within colloidal $CsPbBr_3$ perovskite nanocrystals: remarkably high carrier mobilities and large diffusion lengths. *Nano Lett.* 16, 4838–4848

9. Herz, L.M. (2017) Charge-carrier mobilities in metal halide perovskites: fundamental mechanisms and limits. *ACS Energy Lett.* 2, 1539–1548
10. Chiba, T. *et al.* (2018) Anion-exchange red perovskite quantum dots with ammonium iodine salts for highly efficient light-emitting devices. *Nat. Photonics* 12, 681–688
11. Zhao, X. and Tan, Z. (2020) Large-area near-infrared perovskite light-emitting diodes. *Nat. Photonics* 14, 215–218
12. Lin, K. *et al.* (2018) Perovskite light-emitting diodes with external quantum efficiency exceeding 20 percent. *Nature* 562, 245–248
13. Xu, W. *et al.* (2019) Rational molecular passivation for high-performance perovskite light-emitting diodes. *Nat. Photonics* 13, 418–424
14. Zhao, B. *et al.* (2018) High-efficiency perovskite–polymer bulk heterostructure light-emitting diodes. *Nat. Photonics* 12, 783–789
15. Cao, Y. *et al.* (2018) Perovskite light-emitting diodes based on spontaneously formed submicrometre-scale structures. *Nature* 562, 249–253
16. Lee, T-W *et al.* POSTECH Academy-Industry Foundation. Wavelength converting particle, method for manufacturing wavelength converting particle, and light emitting diode containing wavelength converting particle, US 10424696 B2
17. Lee, T-W *et al.* POSTECH Academy-Industry Foundation. Wavelength converting particle, method for manufacturing wavelength converting particle, and light emitting diode containing wavelength converting particle, KR 1020140153967A
18. Zhang, F. *et al.* (2015) Brightly luminescent and color-tunable colloidal $CH_3NH_3PbX_3$ (X = Br, I, Cl) quantum dots: potential alternatives for display technology. *ACS Nano* 9, 4533–4542
19. Huang, H. *et al.* (2017) Growth mechanism of strongly emitting $CH_3NH_3PbBr_3$ perovskite nanocrystals with a tunable bandgap. *Nat. Commun.* 8, 996
20. Kim, Y.-H. *et al.* (2018) Charge carrier recombination and ion migration in metal-halide perovskite nanoparticle films for efficient light-emitting diodes. *Nano Energy* 52, 329–335
21. Kim, Y.-H. *et al.* (2017) Highly efficient light-emitting diodes of colloidal metal–halide perovskite nanocrystals beyond quantum size. *ACS Nano* 11, 6586–6593
22. Perumal, A. *et al.* (2016) High brightness formamidinium lead bromide perovskite nanocrystal light emitting devices. *Sci. Rep.* 6, 36733
23. Wei, S. *et al.* (2016) Room-temperature and gram-scale synthesis of $CsPbX_3$ (X = Cl, Br, I) perovskite nanocrystals with 50–85% photoluminescence quantum yields. *Chem. Commun.* 52, 7265–7268
24. Yang, Z. *et al.* (2018) Spray-coated $CsPbBr_3$ quantum dot films for perovskite photodiodes. *ACS Appl. Mater. Interfaces* 10, 26387–26395
25. Deng, W. *et al.* (2016) Organometal halide perovskite quantum dot light-emitting diodes. *Adv. Funct. Mater.* 26, 4797–4802
26. Dai, S.W. *et al.* (2018) Perovskite quantum dots with near unity solution and neat-film photoluminescent quantum yield by novel spray synthesis. *Adv. Mater.* 30, 1870048
27. Lee, T-W *et al.* POSTECH Academy-Industry Foundation. Perovskite nanocrystalline particles and optoelectronic device using same, US 10193088 B2
28. Chen, H. *et al.* (2020) High-efficiency formamidinium lead bromide perovskite nanocrystal-based light-emitting diodes fabricated via a surface defect self-passivation strategy. *Adv. Opt. Mater.* 8, 1901390
29. Cho, H. *et al.* (2018) Improving the stability of metal halide perovskite materials and light-emitting diodes. *Adv. Mater.* 30, e1704587
30. Shao, Y. *et al.* (2016) Grain boundary dominated ion migration in polycrystalline organic–inorganic halide perovskite films. *Energy Environ. Sci.* 9, 1752–1759
31. Takagahara, T. and Takeda, K. (1992) Theory of the quantum confinement effect on excitons in quantum dots of indirect-gap materials. *Phys. Rev. B* 46, 15578–15581
32. Li, S.-S. and Xia, J.-B. (2007) Binding energy of a hydrogenic donor impurity in a rectangular parallelepiped-shaped quantum dot: quantum confinement and Stark effects. *J. Appl. Phys.* 101, 93716
33. Steirer, K.X. *et al.* (2016) Defect tolerance in methylammonium lead triiodide perovskite. *ACS Energy Lett.* 1, 360–366
34. Kang, J. and Wang, L.W. (2017) High defect tolerance in lead halide perovskite $CsPbBr_3$. *J. Phys. Chem. Lett.* 8, 489–493
35. ten Brinck, S. and Infante, I. (2016) Surface termination, morphology, and bright photoluminescence of cesium lead halide perovskite nanocrystals. *ACS Energy Lett.* 1, 1266–1272
36. Kim, Y. *et al.* (2019) Bright and uniform green light emitting InP/ZnSe/ZnS quantum dots for wide color gamut displays. *ACS Appl. Nano Mater.* 2, 1496–1504
37. Houtepen, A.J. *et al.* (2017) On the origin of surface traps in colloidal II–VI semiconductor nanocrystals. *Chem. Mater.* 29, 752–761
38. ten Brinck, S. *et al.* (2019) Defects in lead halide perovskite nanocrystals: analogies and (many) differences with the bulk. *ACS Energy Lett.* 4, 2739–2747
39. Baranowski, M. *et al.* (2019) Giant fine structure splitting of the bright exciton in a bulk $MAPbBr_3$ single crystal. *Nano Lett.* 19, 7054–7061
40. Jiang, M. *et al.* (2019) Engineering green-to-blue emitting $CsPbBr_3$ quantum-dot films with efficient ligand passivation. *ACS Energy Lett.* 4, 2731–2738
41. Xu, X. *et al.* (2019) Ultrasonication-assisted ambient-air synthesis of monodispersed blue-emitting $CsPbBr_3$ quantum dots for white light emission. *ACS Appl. Nano Mater.* 2, 6874–6879
42. Yang, D. *et al.* (2019) $CsPbBr_3$ quantum dots 2.0: benzenesulfonic acid equivalent ligand awakens complete purification. *Adv. Mater.* 31, 1900767
43. Li, J. *et al.* (2017) 50-Fold EQE improvement up to 6.27% of solution-processed all-inorganic perovskite $CsPbBr_3$ QLEDs via surface ligand density control. *Adv. Mater.* 29, 1603885
44. Chiba, T. *et al.* (2017) High-efficiency perovskite quantum-dot light-emitting devices by effective washing process and interfacial energy level alignment. *ACS Appl. Mater. Interfaces* 9, 18054–18060
45. Kim, Y.Y. *et al.* (2018) Fast two-step deposition of perovskite via mediator extraction treatment for large-area, high-performance perovskite solar cells. *J. Mater. Chem. A* 6, 12447–12454
46. Zhang, P. *et al.* (2018) Ultrafast interfacial charge transfer of cesium lead halide perovskite films $CsPbX_3$ (X = Cl, Br, I) with different halogen mixing. *J. Phys. Chem. C* 122, 27148–27155
47. Lee, T-W *et al.* POSTECH Academy-Industry Foundation. Method for manufacturing perovskite nanocrystal particle light emitting body where organic ligand is substituted, nanocrystal particle light emitting body manufactured thereby, and light emitting device using same, US 10626326 B2
48. Kim, Y. *et al.* (2017) High efficiency perovskite light-emitting diodes of ligand-engineered colloidal formamidinium lead bromide nanoparticles. *Nano Energy* 38, 51–58
49. Chen, K. *et al.* (2019) Short-chain ligand-passivated stable α-$CsPbI_3$ quantum dot for all-inorganic perovskite solar cells. *Adv. Funct. Mater.* 29, 1900991
50. Dai, J. *et al.* (2018) Charge transport between coupling colloidal perovskite quantum dots assisted by functional conjugated ligands. *Angew. Chem. Int. Ed. Engl.* 57, 5754–5758
51. Vickers, E.T. *et al.* (2018) Improving charge carrier delocalization in perovskite quantum dots by surface passivation with conductive aromatic ligands. *ACS Energy Lett.* 3, 2931–2939
52. Pan, J. *et al.* (2018) Bidentate ligand-passivated $CsPbI_3$ perovskite nanocrystals for stable near-unity photoluminescence quantum yield and efficient red light-emitting diodes. *J. Am. Chem. Soc.* 140, 562–565
53. Li, G. *et al.* (2018) Surface ligand engineering for near-unity quantum yield inorganic halide perovskite QDs and high-performance QLEDs. *Chem. Mater.* 30, 6099–6107
54. Suh, Y.-H. *et al.* (2018) High-performance $CsPbX_3$ perovskite quantum-dot light-emitting devices via solid-state ligand exchange. *ACS Appl. Nano Mater.* 1, 488–496
55. Nag, A. *et al.* (2011) Metal-free inorganic ligands for colloidal nanocrystals: S_2^-, HS^-, Se^{2-}, HSe^-, Te^{2-}, HTe^-, TeS_3^{2-}, OH^-, and NH_2^- as surface ligands. *J. Am. Chem. Soc.* 133, 10612–10620
56. Jo, J.W. *et al.* (2018) Acid-assisted ligand exchange enhances coupling in colloidal quantum dot solids. *Nano Lett.* 18, 4417–4423

57. Song, J. *et al.* (2018) Organic–inorganic hybrid passivation enables perovskite QLEDs with an EQE of 16.48%. *Adv. Mater.* 30, 1–9
58. Woo, J.Y. *et al.* (2017) Highly stable cesium lead halide perovskite nanocrystals through in situ lead halide inorganic passivation. *Chem. Mater.* 29, 7088
59. Hoshi, K. *et al.* (2018) Purification of perovskite quantum dots using low-dielectric-constant washing solvent "diglyme" for highly efficient light-emitting devices. *ACS Appl. Mater. Interfaces* 10, 24607–24612
60. Moyen, E. *et al.* (2018) Ligand removal and photo-activation of $CsPbBr_3$ quantum dots for enhanced optoelectronic devices. *Nanoscale* 10, 8591–8599
61. Kumawat, N.K. *et al.* (2018) Ligand engineering to improve the luminance efficiency of $CsPbBr_3$ nanocrystal based light-emitting diodes. *J. Phys. Chem. C* 122, 13767–13773
62. Moyen, E. *et al.* (2018) Surface engineering of room temperature-grown inorganic perovskite quantum dots for highly efficient inverted light-emitting diodes. *ACS Appl. Mater. Interfaces* 10, 42647–42656
63. Xue, J. *et al.* (2018) Surface ligand management for stable $FAPbI_3$ perovskite quantum dot solar cells. *Joule* 2, 1866–1878
64. Zhang, B. *et al.* (2019) General mild reaction creates highly luminescent organic-ligand-lacking halide perovskite nanocrystals for efficient light-emitting diodes. *J. Am. Chem. Soc.* 141, 15423–15432
65. Li, F. *et al.* (2018) Postsynthetic surface trap removal of $CsPbX_3$ (X = Cl, Br, or I) quantum dots via a ZnX_2/hexane solution toward an enhanced luminescence quantum yield. *Chem. Mater.* 30, 8546–8554
66. Mondal, N. *et al.* (2019) Achieving near-unity photoluminescence efficiency for blue-violet-emitting perovskite nanocrystals. *ACS Energy Lett.* 4, 32–39
67. Zheng, X. *et al.* (2020) Chlorine vacancy passivation in mixed halide perovskite quantum dots by organic pseudohalides enables efficient Rec. 2020 blue light-emitting diodes. *ACS Energy Lett.* 5, 793–798
68. Koscher, B.A. *et al.* (2017) Essentially trap-free $CsPbBr_3$ colloidal nanocrystals by postsynthetic thiocyanate surface treatment. *J. Am. Chem. Soc.* 139, 6566–6569
69. Green, M.L.H. (1995) A new approach to the formal classification of covalent compounds of the elements. *J. Organomet. Chem.* 500, 127–148
70. Nenon, D.P. *et al.* (2018) Design principles for trap-free $CsPbX_3$ nanocrystals: enumerating and eliminating surface halide vacancies with softer Lewis bases. *J. Am. Chem. Soc.* 140, 17760–17772
71. Zhou, Y. and Buhro, W.E. (2017) Reversible exchange of L-type and bound-ion-pair X-type ligation on cadmium selenide quantum belts. *J. Am. Chem. Soc.* 139, 12887–12890
72. Zhong, Q. *et al.* (2019) L-type ligand-assisted acid-free synthesis of $CsPbBr_3$ nanocrystals with near-unity photoluminescence quantum yield and high stability. *Nano Lett.* 19, 4151–4157
73. Cao, W. *et al.* (2017) Halide-rich synthesized cesium lead bromide perovskite nanocrystals for light-emitting diodes with improved performance. *Chem. Mater.* 29, 5168–5173
74. Li, X. *et al.* (2016) $CsPbX_3$ quantum dots for lighting and displays: room-temperature synthesis, photoluminescence superiorities, underlying origins and white light-emitting diodes. *Adv. Funct. Mater.* 26, 2435–2445
75. Ravi, V.K. *et al.* (2017) Origin of the substitution mechanism for the binding of organic ligands on the surface of CsPbBr3 perovskite nanocubes. *J. Phys. Chem. Lett.* 8, 4988–4994
76. Yuan, L. *et al.* (2017) Investigation of anti-solvent induced optical properties change of cesium lead bromide iodide mixed perovskite ($CsPbBr_{3-x}I_x$) quantum dots. *J. Colloid Interface Sci.* 504, 586–592
77. De Roo, J. *et al.* (2016) Highly dynamic ligand binding and light absorption coefficient of cesium lead bromide perovskite nanocrystals. *ACS Nano* 10, 2071–2081
78. Moreels, I. *et al.* (2008) Surface chemistry of colloidal PbSe nanocrystals. *J. Am. Chem. Soc.* 130, 15081–15086
79. Fritzinger, B. *et al.* (2009) *In situ* observation of rapid ligand exchange in colloidal nanocrystal suspensions using transfer NOE nuclear magnetic resonance spectroscopy. *J. Am. Chem. Soc.* 131, 3024–3032
80. Jang, D.M. *et al.* (2015) Reversible halide exchange reaction of organometal trihalide perovskite colloidal nanocrystals for full-range band gap tuning. *Nano Lett.* 15, 5191–5199
81. Zhang, D. *et al.* (2016) Synthesis of composition tunable and highly luminescent cesium lead halide nanowires through anion-exchange reactions. *J. Am. Chem. Soc.* 138, 7236–7239
82. Wong, Y.-C. *et al.* (2019) Color patterning of luminescent perovskites via light-mediated halide exchange with haloalkanes. *Adv. Mater.* 31, e1901247
83. Krieg, F. *et al.* (2018) Colloidal $CsPbX_3$ (X = Cl, Br, I) nanocrystals 2.0: zwitterionic capping ligands for improved durability and stability. *ACS Energy Lett.* 3, 641–646
84. Pan, J. *et al.* (2016) Highly efficient perovskite-quantum-dot light-emitting diodes by surface engineering. *Adv. Mater.* 28, 8718–8725
85. Shin, Y.S. *et al.* (2019) Vivid and fully saturated blue light-emitting diodes based on ligand-modified halide perovskite nanocrystals. *ACS Appl. Mater. Interfaces* 11, 23401–23409
86. Shynkarenko, Y. *et al.* (2019) Direct synthesis of quaternary alkylammonium-capped perovskite nanocrystals for efficient blue and green light-emitting diodes. *ACS Energy Lett.* 4, 2703–2711
87. Park, J.H. *et al.* (2019) Surface ligand engineering for efficient perovskite nanocrystal-based light-emitting diodes. *ACS Appl. Mater. Interfaces* 11, 8428–8435
88. Chen, W. *et al.* (2018) Surface-passivated cesium lead halide perovskite quantum dots: toward efficient light-emitting diodes with an inverted sandwich structure. *Adv. Opt. Mater.* 6, 1800007
89. Krieg, F. *et al.* (2019) Stable ultraconcentrated and ultradilute colloids of $CsPbX_3$ (X = Cl, Br) nanocrystals using natural lecithin as a capping ligand. *J. Am. Chem. Soc.* 141, 19839–19849
90. Imran, M. *et al.* (2019) Simultaneous cationic and anionic ligand exchange for colloidally stable $CsPbBr_3$ nanocrystals. *ACS Energy Lett.* 4, 819–824
91. Yassitepe, E. *et al.* (2016) Amine-free synthesis of cesium lead halide perovskite quantum dots for efficient light-emitting diodes. *Adv. Funct. Mater.* 26, 8757–8763
92. Tan, Y. *et al.* (2018) Highly luminescent and stable perovskite nanocrystals with octylphosphonic acid as a ligand for efficient light-emitting diodes. *ACS Appl. Mater. Interfaces* 10, 3784–3792
93. Sun, H. *et al.* (2017) Chemically addressable perovskite nanocrystals for light-emitting applications. *Adv. Mater.* 29, 1701153
94. Ruan, L. *et al.* (2017) Stable and conductive lead halide perovskites facilitated by X-type ligands. *Nanoscale* 9, 7252–7259
95. Song, J. *et al.* (2015) Quantum dot light-emitting diodes based on inorganic perovskite cesium lead halides ($CsPbX_3$). *Adv. Mater.* 27, 7162–7167
96. Huang, H. *et al.* (2015) Emulsion synthesis of size-tunable $CH_3NH_3PbBr_3$ quantum dots: an alternative route toward efficient light-emitting diodes. *ACS Appl. Mater. Interfaces* 7, 28128–28133
97. Leijtens, T. *et al.* (2017) Mechanism of tin oxidation and stabilization by lead substitution in tin halide perovskites. *ACS Energy Lett.* 2, 2159–2165
98. Luo, J. *et al.* (2018) Efficient and stable emission of warm-white light from lead-free halide double perovskites. *Nature* 563, 541–545
99. Locardi, F. *et al.* (2018) Colloidal synthesis of double perovskite $Cs_2AgInCl_6$ and Mn-doped $Cs_2AgInCl_6$ nanocrystals. *J. Am. Chem. Soc.* 140, 12989–12995
100. Kayanuma, Y. (1988) Quantum-size effects of interacting electrons and holes in semiconductor microcrystals with spherical shape. *Phys. Rev. B* 38, 9797–9805
101. Kayanuma, Y. (1986) Wannier exciton in microcrystals. *Solid State Commun.* 59, 405–408

102. Einevoll, G.T. (1992) Confinement of excitons in quantum dots. *Phys. Rev. B* 45, 3410–3417
103. Jang, H.M. *et al.* (2020) Enhancing photoluminescence quantum efficiency of metal halide perovskites by examining luminescence-limiting factors. *APL Mater.* 8, 20904
104. Li, G. *et al.* (2016) Highly efficient perovskite nanocrystal light-emitting diodes enabled by a universal crosslinking method. *Adv. Mater.* 28, 3528–3534
105. Chin, X.Y. *et al.* (2018) Self-assembled hierarchical nanostructured perovskites enable highly efficient LEDs via an energy cascade. *Energy Environ. Sci.* 11, 1770–1778
106. Lu, M. *et al.* (2018) Spontaneous silver doping and surface passivation of $CsPbI_3$ perovskite active layer enable light-emitting devices with an external quantum efficiency of 11.2%. *ACS Energy Lett.* 3, 1571–1577
107. Di, D. *et al.* (2015) Size-dependent photon emission from organometal halide perovskite nanocrystals embedded in an organic matrix. *J. Phys. Chem. Lett.* 6, 446–450
108. Berestennikov, A.S. *et al.* (2019) Beyond quantum confinement: excitonic nonlocality in halide perovskite nanoparticles with Mie resonances. *Nanoscale* 11, 6747–6754
109. Dong, Y. *et al.* (2020) Bipolar-shell resurfacing for blue LEDs based on strongly confined perovskite quantum dots. *Nat. Nanotechnol.* 15, 668–674